Silicon-Organic-Hybrid Independent Simultaneous Dual-Polarization Modulator: Device Theory and Design

Yannick D'Mello*[1], Michael Hui[1], James Skoric[1], Matthew Haines[1], Andrew Kirk[1], Mark Andrews[2], and David Plant[1]
1. Department of Electrical and Computer Engineering, McGill University, Montreal, Canada
2. Department of Chemistry, McGill University, Montreal, Canada
*Yannick.DMello@mail.McGill.ca

The linear electro-optic Pockels effect induces an effective refractive index change in non-centrosymmetric optical materials. Its sub-picosecond response time and low energy requirement are attractive characteristics towards using this effect as a phase modulation scheme. This paper investigates the characteristics of a device that is capable of modulating the fundamental mode of two orthogonal polarizations separately and simultaneously. The device exploits both dimensions in the birefringent response of thermally poled Electro-Optic Polymers (EOP) when inducing a polarization dependent Pockels effect. A characterization of this behavior is carried out for a polymethylmethacrylate (PMMA) matrix with DR1 or CLD1 chromophores in a guest-host structure. This path offers improvements in energy consumption and speed due to the utilization of the Pockels effect, as well as added functionality from its incorporation of polarization-division multiplexing.

Index Terms—electro-optic polymer (EOP), phase modulation, photonics, Pockels effect.

I. Introduction

The implementation of photonics in telecommunication architecture has significantly increased the bandwidth of current data communications, and motivated progress in throughput, latency and efficiency. This is motivated by a push towards increasingly high-speed and high-bandwidth devices at low costs as a direct response to global demand [1]. In order to cater to this need, smarter signal processing tools are designed to employ multiple degrees of freedom (frequency, polarization/mode, phase, amplitude) within the same signal therefore compounding the data carrying capacity of networks. Regarding the transmission and reception ends, significant emphasis is placed on improving modulation and multiplexing schemes with a view to increasing size, speed, or efficiency within devices [2].

The current industry standards for modulators make use of various optical phenomena to modulate a propagating signal. For example, the Franz-Keldysh effect [3] is used in electro-absorption modulators; the plasma dispersion effect in phase modulators [4]; as well as other effects such as the acousto-optic effect [5] for frequency shifting, or electro-optic effect [6] for phase shifting. Lithium Niobate ($LiNbO_3$) is a commonly used nonlinear optical material for fiber-based modulators due to its optical transparency in the telecom wavelength range and high bandwidth, obtained through the implementation of the electro-optic effect [7]. However, the integration of $LiNbO_3$ in CMOS-compatible systems can be challenging. An interesting alternative is found as an application of polymer chemistry. Electro-optic polymers undergo an isochoric change in their electromagnetic properties, such as refractive index, upon application of an electric field. This change is caused by a bulk electro-optic effect from the overall dipole orientation of chromophores within the polymer, known as the Pockels effect [8].

II. Theory

The Pockels effect is a second-order nonlinear optical effect that is dependent on the polarizability of a material – inherent and induced. It is referred to as a linear electro-optic effect of the first order because the resultant change in refractive index P/E varies linearly with the applied electric field [8],

$$\Delta n \propto \frac{\vec{P}}{\vec{E}} \propto n_0 + r_{ijk}\vec{E} + \cdots \qquad (1)$$

Here, Δn represents an induced change in refractive index caused by an applied external field $\vec{E}$ on a material with initial refractive index n_0 and a linear electro-optic tensor r_{ijk} that determines its electro-optic responsivity to the applied electric field. Although the optical response time correlates with the mobility of electrons, this response is quick enough (sub-picosecond regime) that the electro-optic coefficient can be considered independent of the

1

magnitude and modulation frequency of the applied field [8].

An applied field implicitly interrogates every nonlinear term associated with a material. However, it is possible to enhance the inherent $\chi^{(2)}$ of an EOP through thermal poling which results in an amplified Pockels effect [6]. Through the process of thermal poling, the dipole orientation of the chromophores within the EOP lose their rigidity when heated to the glass transition temperature so that they can align to an externally applied electric field. Due to the uniaxial orientation of the poled EOP chromophores, the effective nonlinear coefficients are stronger for any propagating light that is polarized such that its oscillating electric field is parallel to the poled dipole orientation. In this manner, a birefringence is induced in the EOP molecules as depicted in Figure 1.
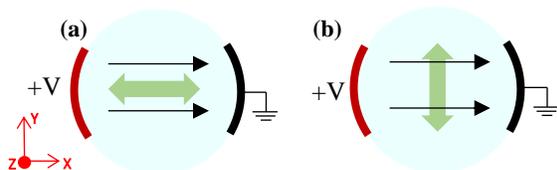

Figure 1: Electric polarization of an EOP under an applied electric field. The thick lines represent the electrodes, the black arrows show the induced electric moment and the green arrow indicates the oscillation of the electric field of polarized light propagating down the Z axis. In (a), the molecular electric moments oriented along the positive X axis will interact directly with TE polarized light (E-field parallel to X axis) since they are parallel, whereas in (b), the induced moment only weakly interacts with TM polarized light (E-field parallel to Y axis). Hence, orthogonal polarizations of the optical signal propagating through a thermally poled EOP will experience significantly different refractive indices.

Poling imposes a cylindrical point group symmetry with the axis parallel to the poling field. This point group symmetry reduces r_{ijk} to r_{mk} thus restricting the tensor to three independent elements, which correspond to the dipole orientation along the X, Y and Z axes [6],

$$r_{ijk} \rightarrow r_{mk} = \begin{bmatrix} 0 & 0 & r_{13} \\ 0 & 0 & r_{13} \\ 0 & 0 & r_{33} \\ 0 & r_{31} & 0 \\ r_{31} & 0 & 0 \\ 0 & 0 & 0 \end{bmatrix} \qquad (2)$$

As determined by the electro-optic coefficient tensor, the application of an electric field causes a proportional variation in refractive index, which differs for polarizations that are parallel or perpendicular to the $\vec{E}$ vector. For example, poling along the direction of polarization induces a change in refractive index that can be approximated by [6],

$$n_i(E) = n_0 - \frac{1}{2}r_{33}n_0^3 E_i \qquad (3)$$

Where n_0 denotes the original effective refractive index of the EOP waveguide. If, however, the polymer is poled perpendicular to the direction of polarization, the induced change in refractive index will be given by,

$$n_i(E) = n_0 - \frac{1}{2}r_{31}n_0^3 E_j$$
$$\text{or} \qquad (4)$$
$$n_i(E) = n_0 - \frac{1}{2}r_{13}n_0^3 E_k$$

depending on the direction of the applied electric field. The oriented gas model is chosen to estimate the relationship between the elements of the tensor, and it predicts that $r_{33} = 3r_{13}$. Additionally, the Kleinman symmetry approximation has been used to set $r_{13} \approx r_{31}$ and is partially based on experimental confirmation [9]. These degrees of freedom will be exploited in our design of a dual polarization EOPM.

III. Device Design

As discussed in the previous section, the orientation of the chromophores with respect to the polarization of incident light determines the refractive index response. In order to interrogate the r_{33} and r_{13} coefficients for polarized light propagating along the Z-axis through a cylindrical waveguide, it must be possible to apply an electric field along either the X or Y axes. This is made possible by using four opposing electrodes as shown in Figure 2.
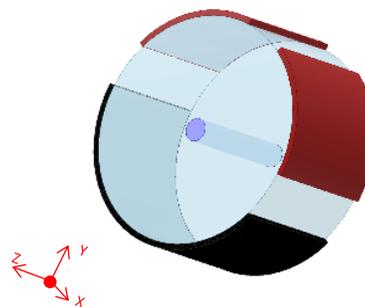

Figure 2: Three-dimensional view of proposed configuration for dual polarization modulation. The signal electrodes are represented in red and ground electrode in black. As both ground electrodes are electrically equivalent, they are considered to be a single electrode so as to reduce fabrication complexity. The EOP core is shown in blue, and surrounded by concentric glass cladding.

The dual-polarization electro-optic modulator (DP-EOPM) was designed using two different chromophores. DR1 is used as a reference EOP seeing as its nonlinear properties have been comprehensively

2

explored and are well understood [9]. However, as its r_{33} coefficient is very low, it is no longer used in practical applications. As an alternative, CLD1 has a significantly higher Pockels coefficient [10] making it a suitable candidate for future experimental verification. PMMA was used as the host matrix in both cases to maintain consistency. The parameters for these two polymers are given in Table 1.

Parameter		DR1/ PMMA	CLD1/ PMMA
Refractive Index	n_{co}	1.475	1.63
Pockels coeff. [pm/V]			
On-axis	r_{33}	7.6	85
Off-axis	r_{31}	2.9	28.33*
Wt. percent in PMMA	wt%	10	10

*Estimated using $r_{33} = 3r_{31}$ as defined in section II

Table 1: Characteristics of DR1/PMMA and CLD1/PMMA using [6][8][9][10].

The percent weight ratio was used to calculate the bulk refractive index of the material [8]. The characterization of DR1/PMMA was extensively performed in [9], which experimentally investigated the $C_{\infty m}$ point group symmetry. This allows the numerical work to be simplified by considering an average of the electro-optic tensor elements r_{42} and r_{51} such that $r_{42}, r_{51} \approx r_{31} \approx 2.9$ pm/V. It has also been assumed that the initial (unpoled) extraordinary and ordinary refractive indices are approximately equal, as represented by n_0. Hence the change in refractive index along the X- and Y-axis as a result of applying electric fields along the X- and Y-axes respectively, can be reduced to,

$$n_x(E) = n_{0,x} - \frac{1}{2}r_{33}n_{0,x}^3 E_x$$
$$n_y(E) = n_{0,y} - \frac{1}{2}r_{33}n_{0,y}^3 E_y \quad (5)$$

In order to produce an intensity variation, the DP-EOPM must be placed in a Mach-Zehnder Interferometer configuration in which a π phase shift will be required. As the phase shift is a function of the change in refractive index induced by the applied electric field, the half wave voltage V_π across the electrodes that is required to produce this phase shift is given by,

$$V_\pi = \frac{\lambda d}{n^3 r_{eff} L \Gamma} \quad (6)$$

Here, the central wavelength λ is 1.55μm, d is the distance between electrodes, L is the interaction length, and Γ is the overlap integral as determined by the vectorial overlap between the signal applied electric field and the confined beam profile. If the applied electric field is parallel to the confined beam at all points, $\Gamma = 1$, and if it is antiparallel, $\Gamma = -1$. In the case of crossed beams, $\Gamma = 0$ as this is taken into account in the overlap integral for r_{31}. Thus perpendicular electric field is susceptible to the r_{31} coefficient requiring an expansion of the half-wave voltage equation,

$$V_\pi = \left(\frac{1}{r_{33}\Gamma_{on-axis}} + \frac{1}{r_{31}\Gamma_{off-axis}} \right) \frac{\lambda d}{n^3 L} \quad (7)$$

IV. Simulation Setup

Regarding the propagation of two orthogonal, linear polarizations through the cylindrical EOP core under an externally applied electric field, the overlap criteria must be determined. This implies the determination of the vectorial components of the applied electric field, as well as the beam profile of the fundamental modes propagating through the core.

a. Signal Electric Field

An initial two-dimensional electrostatic and electromagnetic simulation was performed along the cross-section of the proposed structure. This simulation uses the AC/DC > Electrostatic (es) and Optics > Wave Optics > Electromagnetics Waves, Frequency Domain (ewfd) modules. The diameter of the cross-section is $20\mu m$ with a uniform dielectric constant approximation, corresponding to glass. Two signal electrodes are positioned on the left (X-axis) and top (Y-axis), and one uniform ground electrode covers both the right (X-axis) and bottom (Y-axis) with corresponding spacing. The ground electrode therefore complements each signal electrode. Figure 3 below illustrates the static electric field when the same positive potential is applied to both signal electrodes.
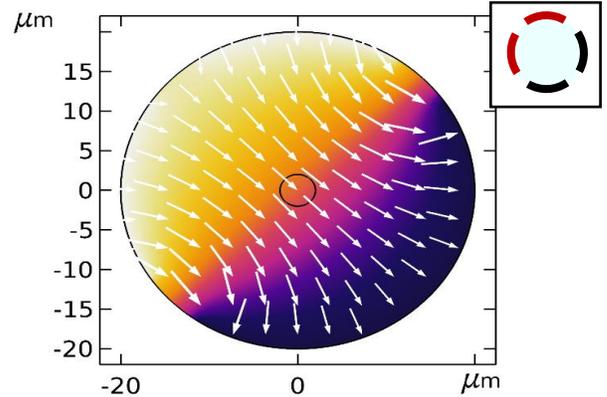

Figure 3: Applied electric field distribution along a cross-section of the EOPM with both electrodes active and (inset) corresponding electrode map using the format depicted in Figure 1.

3

The vectorial distribution portrays the directional nature of the electric field along the cross-section of the cylindrical waveguide. As can be seen, a cladding region between electrodes and waveguide core provides a separation between the maximum intensity of the beam profile and the signal field. This separation effectively straightens the electric field through the core, ensuring that it is the intended vectorial sum of both signals. Thus fringe effects between electrodes has been neglected [11]. When a positive voltage is applied to both signal electrodes, the effective angle of the applied external electric field at the core is almost uniformly 45° allowing for an equivalent modulation of both propagating polarizations.

b. Mode Confinement

The parameters used to determine the confinement of both polarizations within the EOP core are given in Table 2. These parameters are used to simulate the fundamental mode using COMSOL while neglecting the ordinary and extraordinary refractive index differences as explained in section III.

Parameter	Value
$n_{DR1/PMMA}$	1.475
$n_{CLD1/PMMA}$	1.63
n_{clad}	1.47
r_{core}	$2\ \mu m$
r_{clad}	$20\ \mu m$

Table 2: Waveguide parameters for DR1/PMMA and CLD1/PMMA EOP cores with a borosilicate glass cladding, at a propagating wavelength of 1550nm [9][10].

Analytically, the parameters for DR1/PMMA in Table 2 will only support the fundamental mode in the proposed waveguide since $\frac{2\pi r_{core}}{\lambda}\sqrt{n_{core}^2 - n_{clad}^2} <$ 2.405 [12]. Although increasing the core refractive index with the use of CLD1/PMMA permits higher-order mode as predicted by the dispersion equation [12], the fundamental mode can still be analyzed and compared against DR1/PMMA. Using 'Mode Analysis' with 'ewfd' in COMSOL, the parameters in Table 2 were simulated to obtain the beam profiles shown in Figure 4.
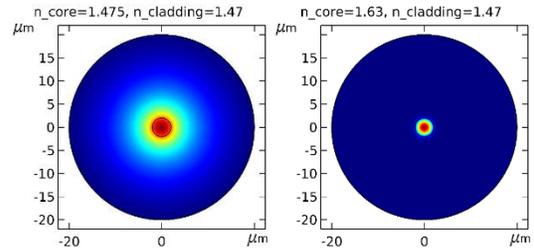

Figure 4: Fundamental mode profiles for CL1/PMMA (left) and DR1/PMMA (right).

A vector product of the linearly polarized mode profile, and applied electric field, is used to calculate the effective overlap. This overlap indicates the efficiency of the applied field on phase modulation of light through the polymer. In typical EOP modulators, the optical confinement is considerably greater through the use of high-index polymers [13] or slot waveguides [14], thereby increasing the effective overlap. For the purpose of simplicity, these techniques have not been incorporated and hence much lower efficiencies (and correspondingly higher interaction lengths) are expected. A 3D simulation is carried out to determine the modulation characteristics of this structure.

c. Three-Dimensional Propagation Set-up

The simulation set-up described above was further extended to a three-dimensional cylindrical waveguide. The fiber model is 8mm long and consistent with the parameters in Table 1 and Table 2. The waveguide length was specifically restricted to 8mm with the interest of conserving simulation time. This is justified by the predictability of the optical response since the magnitude of phase change (with respect to the original wave) is expected to be linearly increasing as the wave propagates through the fiber. As shown in the equation below, the electro-optic phase change is linearly proportional to waveguide interaction length, L [15].

$$|\Delta\varphi| = \frac{rn^3EL}{\lambda_0} \qquad (8)$$

In preparation for the 3D model construct in COMSOL, the 'Electromagnetic Waves, Beam Envelope (ewbe)' module was used instead of the 'Electromagnetic Waves, Frequency Domain (ewfd).' In order to excite 45° (diagonally) polarized light into the fiber, a 'User Defined' port was chosen instead of the typical choice of 'Numeric' port. This enables the specification of the X and Y components of the port's $e^{j\beta z}$ fields, thereby allowing the input field into waveguide to be diagonally linearly polarized. Considering the modulation target of a π-phase shift, a 'Matched Boundary Condition' was used as opposed

4

to defining a terminating port; this suggests that the modulator extends beyond the simulated structure, which prevents unintended terminations (i.e. defining a listener port – Port 2) and corresponding back reflections. A scattering boundary condition was also applied to the waveguide structure to indicate that the surrounding environment is air.

Regarding the coupled electrostatic field as calculated within the 'Electrostatics (es)' module, a similar configuration is performed for the 3D structure as that used in the 2D simulation. The electrodes are specified as applied potentials on the top and side. The same technique is used to place a uniform grounding electrode on opposing sides of the electric potential.

The effective index was extracted from the 'Derived Values > Global Evaluation' section in the 2D simulation to allow for a comparison against the results obtained in the 3D simulation, which uses a 'Numeric' port.

V.   Simulation Results

The 3D device characteristics are predicted for certain key parameters. As phase modulation is the target application of this system, the optical response metric of the device is considered to be the induced phase shift in radians.

An applied signal along one electrode axis is expected to affect the refractive index experienced along that axis itself, and not necessarily the perpendicular axis. However, as shown in the 2D simulation of electric field in Figure 3, a minor crosstalk results due to the electrostatic field angles at the core deviating slightly from 45° when both electrode sets are being used. A more severe source of crosstalk due to the static electric field arises from the off-axis electro-optic coefficient that induces a phase shift in the polymer. Crosstalk is expected to accumulate as the optical wave propagates down the interaction length of the electro-optical material. Figure 5 illustrates the simulated result when a voltage of 10V is applied along the X-axis, and induces approximately $\frac{\pi}{2}$ phase shift along the horizontal axis while imposing an approximately $\frac{\pi}{6}$ phase shift along the vertical axis. The large electro-optic coefficient of CLD-1/PMMA facilitates a much smaller interaction length as compared to DR1 for the same resultant phase shift. As the phase shift measured is a relative quantity that is referenced with the initial phase and a function of the periodic wavelength, the phase shift as well is expected to be periodic over large interaction lengths.
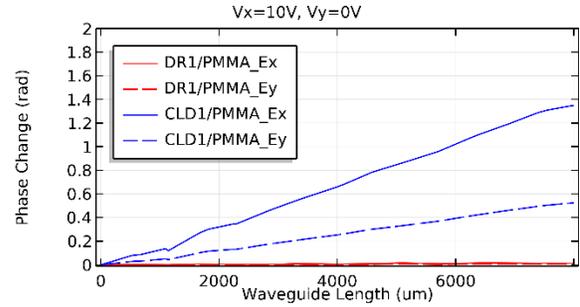

Figure 5: Phase shift in propagating X-polarized light (E_x) as a function of waveguide length when only the X-axis electrode is active, and corresponding static phase shift induced in orthogonally polarized (E_y) light.

For a modulator with constrained dimensions, it is expected that CLD1 would require a lower voltage to obtain an equivalent phase shift as DR1 at the same interaction length. Alternatively, increasing the voltage will increase the amount of phase shift experienced by the propagating light; similar to any single polarization modulator. Since the magnitude of phase change is linearly proportional to the applied potential, it can be extracted from Figure 6 that a voltage of approximately 20V for a waveguide length of 8mm can achieve a π-phase shift using CLD1/PMMA, considering the simplistic modulator structure designed in section III.
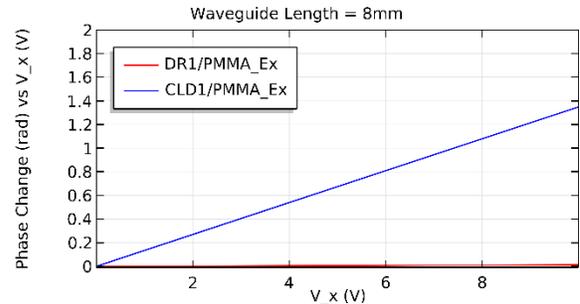

Figure 6: Phase change as a function of applied voltage along the X-axis.

Although the static off-axis phase shift induced by an electrode set is relatively strong, the effect of both electrodes being used simultaneously proves the ability to modulate both polarizations within the same structure. From Figure 7, it can be seen that the orthogonal electric fields from the dual polarization modulators are affected equally for applied voltages of 10V for X- and Y-axes. As a result, the magnitude of phase shift for both orthogonal fields is nearly identical. It is seen that the calculated phase change for dual polarization modulation is higher than a single axis modulation due to the incumbent phase shift as a result of the magnitude of the diagonal component being stronger than each orthogonal component, as

5

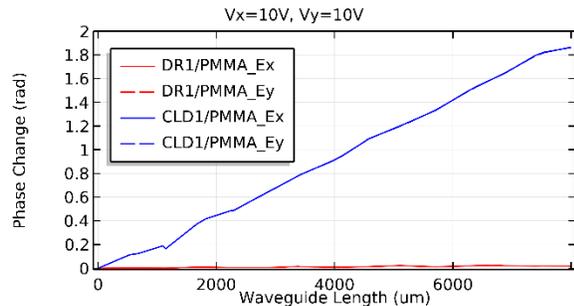well as the residual phase shift from off-axis components.

Vx=10V, Vy=10V

Figure 7: Phase change as a function of waveguide length when both electrodes are active.

VI. Conclusion

We report the concept, design and simulation of a dual polarization electro-optic polymer modulator for optical phase modulation applications. The device structure consists of concentric EOP core, glass cladding, and four radially symmetric electrodes, along the axis of propagation for linearly polarized light. Simulation results show an effective phase shift of 1.35 radians for CLD1 and 0.01 radians for DR1 under a 20V applied voltage with an interaction length of 8mm. Additionally, static crosstalk is expected to be approximately a third of the induced phase shift in any scenario. Such a device allows the option of simultaneously modulating two phases within a single structure at an extremely high speed and theoretically low voltage, and thus offers a solution to the speed, size, and efficiency constraint imposed on modulators in contemporary telecommunication architecture.

VII. References

[1] Chrostowski, Lukas, and Michael Hochberg. *Silicon photonics design: from devices to systems.* Cambridge University Press (2015).

[2] Thomson, David, et al. "Roadmap on silicon photonics." *Journal of Optics* 18.7, 073003 (2016).

[3] Seraphin, B. O., and N. Bottka. "Franz-Keldysh effect of the refractive index in semiconductors." *Physical Review,* 139.2A, A560 (1965).

[4] Patel, David. *Design, Analysis, and Performance of a Silicon Photonic Traveling Wave Mach-Zehnder Modulator.* Masters Diss. McGill University (2014).

[5] Kim, B. Y., et al. "All-fiber acousto-optic frequency shifter." *Optics Letters* 11.6, 389-391 (1986).

[6] Günter, Peter, ed. *Nonlinear optical effects and materials.* Vol. 72. Springer (2012).

[7] Wooten, Ed L., et al. "A review of lithium niobate modulators for fiber-optic communications systems." *IEEE Journal of selected topics in Quantum Electronics* 6.1**,** 69-82 (2000).

[8] Zerbi, Giuseppe, ed. *Organic Materials for Photonics: Science and Technology*. Elsevier (1993).

[9] Sugita, Atsushi, et al. "Second-order nonlinear optical susceptibilities of nonelectrically poled DR1–PMMA guest–host polymers." *The Journal of Physical Chemistry B* 117.47, 14857-14864 (2013).

[10] Zhang, Cheng, et al. "Low Vπ electrooptic modulators from CLD-1: chromophore design and synthesis, material processing, and characterization." *Chemistry of materials* 13.9, 3043-3050 (2001).

[11] Sadiku, Matthew. *Elements of electromagnetics.* Oxford university press (2014).

[12] Okamoto, Katsunari. *Fundamentals of optical waveguides*. Academic press (2010).

[13] Li, Ming, et al. "Poling efficiency enhancement of tethered binary nonlinear optical chromophores for achieving an ultrahigh n3 r33 figure-of-merit of 2601 pm V− 1." *Journal of Materials Chemistry C*3.26, 6737-6744 (2015).

[14] Almeida, Vilson R., et al. "Guiding and confining light in void nanostructure." *Optics letters* 29.11, 1209-1211 (2004).

[15] Bass, Michael, et al. *Handbook of Optics.* McGraw-Hill (2009).

VIII. Acknowledgements